ORIGINAL ARTICLE

lajss.org© Latin American Journal of Solids and Structures

www.lajss.org

Kinetic response of reinforced concrete slabs to high-velocity projectile impact-robust numerical and statistical driven modeling techniques

Ammar Babiker[a], Yassir M. Abbas[b*], M. Iqbal Khan[b], Jamal M. Khatib[c]

[a] School of Civil Engineering, College of Engineering, Sudan University of Science and Technology, P.O. Box 72, Eastern Daim, Khartoum, Sudan. Email: ammar.babiker@sustech.edu

[b] Department of Civil Engineering, College of Engineering, King Saud University, P.O. Box 800, Riyadh -11421, Saudi Arabia. Email: yabbas@ksu.edu.sa, miqbal@ksu.edu.sa

[c] Faculty of Science and Engineering, University of Wolverhampton, Wolverhampton WV1 1LY, UK. Email: j.m.khatib@wlv.ac.uk

* Corresponding author

https://doi.org/10.1590/1679-78258009

Abstract

This research explores the dynamic responses of reinforced concrete (RC) slabs under high-velocity impacts. The study utilizes advanced numerical simulations to investigate the effects of varied impact loading and slab depths, unveiling complex rate-dependent behaviors (i.e., impact forces, reactions, accelerations, and displacements) across a diverse range of velocities. The alignment of simulation results with experimental data validates the robustness and accuracy of the employed approach. Additionally, an analytical model predicting the load-carrying capacity and deflection of these slabs under high-velocity loads is proposed. The results indicated that higher loading rates correlate with increased forces and damage until perforation. Analytical models exhibit strong performance within a ±10% error margin, and response surface analysis quantifies the impactor velocity's influence on load for a constant thickness. Overall, this investigation sheds light on the dynamic complexities of RC slabs subjected to high-velocity impacts, providing valuable insights for structural design considerations.

Keywords

Impact loading, Reinforced Concrete, Slabs, Drop-tower, Material model, LS-Dyna.

Graphical Abstract

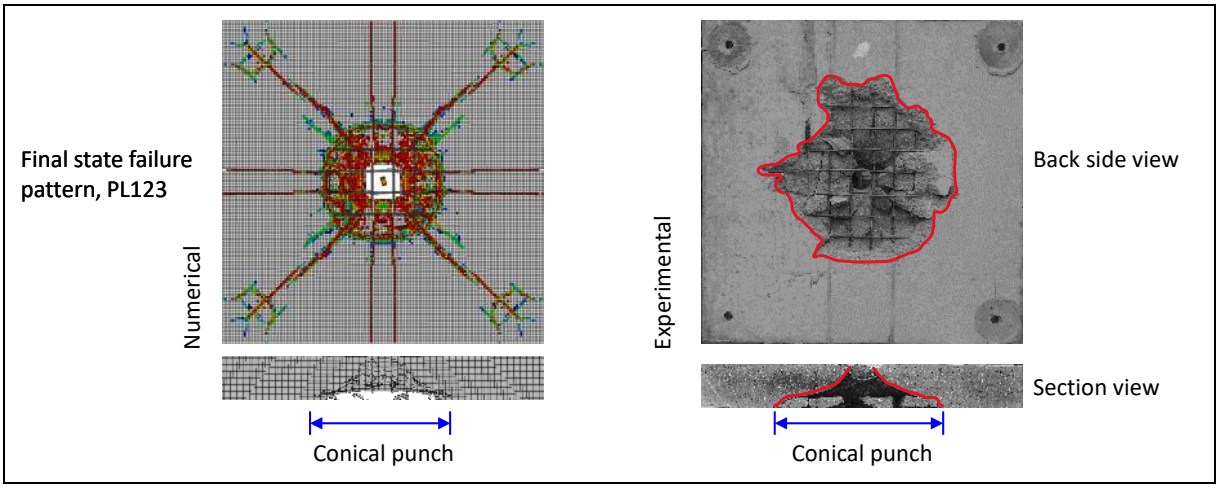

Received January 25, 2024. In revised form January 31, 2024. Accepted February 12, 2024. Available online February 15, 2024.
https://doi.org/10.1590/1679-78258009

Latin American Journal of Solids and Structures. ISSN 1679-7825. Copyright © 2024. This is an Open Access article distributed under the terms of the Creative Commons Attribution License, which permits unrestricted use, distribution, and reproduction in any medium, provided the original work is properly cited.

INTRODUCTION

Background

The versatility and importance of Reinforced concrete (RC) as a construction material are widely attested by its ability to withstand extreme loading conditions, including impact from projectiles, vehicles, aircraft, and debris. Several factors influence the impact resistance of reinforced concrete structures, including the density of the material, the configuration of the reinforcement, the characteristics of the projectile, and the boundary conditions at the time of impact (Andrew et al. 2019; Dhiman, P., Kumar 2023; Tai et al. 2011; J. Liu et al. 2023). It is therefore crucial to understand the behavior and failure modes of RC structures under impact loading, as well as to develop reliable numerical methods to simulate and predict their response under impact loading to develop reliable designs.

Numeral analysis involves algorithms that solve problems in mathematics through numerical approximations, including differential equations, linear algebra, optimization, and interpolation. Deformation and damage to RC structures under impact loading can be modeled numerically using continuous variables (Fan et al. 2022; J. Liu et al. 2023; Othman and Marzouk 2017). RC structures under impact loading present some challenges during the numerical analysis of the structure, including the need to account for nonlinear and dynamic characteristics of the materials within the structure as well as the effect of the loading (Richard et al. 2016; Quan et al. 2003; Karagöz İşleyen et al. 2023). As a heterogeneous and brittle material, concrete is susceptible to strain rate effects such as cracking, crushing, and spalling as a result of high strain rates (Zhang et al. 2021; Hao, Zhang, and Hao 2011; Erzar and Forquin 2011). As well as its ductility, mild steel reinforcement can exhibit strain-rate effects, yielding, and fracture phenomena at high-stress levels (Cadoni et al. 2013; Chandran et al. 2022). The binding and slipping behavior between concrete and steel reinforcement is determined by bond-slip behavior, which can have a profound effect on load transfer and energy dissipation (Bencardino, Condello, and Ashour 2017; Sahani and Samanta 2022; Deng et al. 2022). The impact scenario may cause the structure to experience large deformations, vibrations, and global or local failure modes, as a result of its deformations.

Bibliographical overview

The dynamic loading-induced response of both concrete and reinforced concrete (RC) structures has garnered substantial attention in both civilian and military applications. Extensive research has been dedicated to investigating the impact behavior of reinforced concrete, encompassing not solely empirical investigations but also analytical and numerical inquiries (Bruhl, Varma, and Johnson 2015; Hering and Curbach 2018; Hering et al. 2020; Lu, Li, and Wang 2012; Daudeville and Malécot 2011; Korucu and Irfanoglu 2018). Within this framework, a multitude of factors, including but not limited to compressive strength, tensile strength, fracture energy, strain-rate sensitivity, impact velocity, target geometry, and impactor properties, have been meticulously examined and recognized as pivotal elements influencing the structural response to dynamic loading (Chen et al. 2007; 2008).

Additionally, Bruhl et al. (Bruhl, Varma, and Johnson 2015) outlined a three-step method for designing steel plate composite (SC) walls to prevent perforation by missile impact. It calculates the required steel plate thickness for SC walls to resist a realistic range of missile threats. Additionally, the paper introduces 3D finite element models to predict SC wall behavior during missile impact and validates them through parametric studies. Hering and Curbach (Hering and Curbach 2018) presented an innovative testing approach aimed at identifying the optimal fabric reinforcement for enhancing the impact resistance of reinforced concrete structures. A comparison is made between the different velocities of Textile Reinforced Concrete (TRC) and conventional concrete slabs. The study's findings highlight that the disparity in velocity could function as an evaluative metric for gauging the impact resistance of fabric used in slab reinforcement. Lu et al. (Lu, Li, and Wang 2012) reported numerical simulations of rigid projectile impacts hitting plain concrete and fiber-reinforced concrete targets with compressive strengths ranging from 45 to 235 MPa. The study utilized a combined dynamic constitutive model to study concrete damage due to compressive and tensile forces. The prediction of this study highlighted that as the projectile moves at high speed, an extrusion dilation of the target material is observed early in the penetration process. It was also found that with increasing penetration depths and decreasing projectile speeds, damage zones gradually reduce. Furthermore, the study demonstrated that tensile damage distributes around the impact center, whereas compression damage becomes prominent near the projectile and it is vicinity. In Daudeville and Malecot (Daudeville and Malécot 2011) the paper focused on identifying the response of concrete structures subjected to impulsive loading such as impact. The study examined a wide range of existing basic relations and empirical formulas. The study indicated that according to experimental analyses of concrete behavior under high triaxial stresses, empirical formulas should be used with caution. Despite a limited understanding of material behavior in this range of loading, the paper emphasizes the need for analytical treatments comparable to those for structures under static loading. Using finite

element (FE) and Smooth Particles Hydrodynamics (SPH), Korucu and Irfanoglu (Korucu and Irfanoglu 2018) applied a fluid-filled projectile with various velocities on reinforced concrete beams featuring either rectangular or circular transverse reinforcements to study and assess the reliability of the numerical modeling and simulation technique to verify the ability to reasonably estimate damage inflicted by fluid impact. The results demonstrated that the beams with spiral transverse reinforcement exhibited much better performance. The study also highlighted that at low-impact velocities, the residual velocities of the projectile after perforation exhibited no significant differences between the rectangular and circular specimens. Chen et al. (Chen et al. 2007; 2008) adopted an analytical model for the normal perforation of reinforced concrete slabs by rigid projectiles. In the model, reinforcing bars are taken into account and three dimensionless numbers are used, including impact, geometry, and concrete thickness. In addition, the concrete reinforcement ratio and the reinforcing bar tensile strength are considered to influence the process of perforation. A comparison of the crater dimensions of the theoretical predictions of the model and the experimental ones indicated that the analytical model can well capture the perforation of RC slabs. The model also demonstrated a higher degree of accuracy compared to other proposed models, for instance, Dancygier (Dancygier 1997). Using inclined reinforcement in reinforced concrete slabs, Vijay et al. (Vijay et al. 2020) carried out an investigation aimed at enhancing the understanding of their impact behavior. It emphasizes the importance of investigating the impact behavior of RC slabs embedded with non-conventional reinforcement patterns. The study provides experimental evidence that inclined reinforced RC slabs can absorb higher impact energy and withstand significant impact factors for longer periods than conventional slabs. Gomathi et al. (Gomathi et al. 2020) introduced a plasticity-based approach for reinforced concrete slabs exposed to impact and blast loading. A new failure surface is proposed along with a modified equation of state (EOS), strain rate, and damage. The model was implemented utilizing a user-defined UMAT subroutine of LS-Dyna finite element software. Both impact and blast analysis demonstrate the effectiveness of the proposed approach. Furthermore, the study conducted a systematic analysis, varying parameters like concrete strength, slab thickness, and reinforcement ratio, to scrutinize mechanical and damage responses. Overall, the study introduces an innovative approach for analyzing the dynamic response of RC slabs under impact and blast loads, offering insights applicable to the design of structures engineered to endure such load conditions.

Scope and significance of the research

This research explores the impact of high-velocity projectiles on RC slab structural behavior. In particular, this research aims to provide a deeper understanding of the failure mechanisms and performance of these structures under extreme loading conditions. The results of this study may contribute valuable insight into both civilian and military contexts. The knowledge gained from this research could enable civil infrastructure to be designed and built in a more durable and ductile manner to withstand the impact of unforeseen projectiles. Further, it would be possible to use the findings to develop protection measures for structures exposed to high-velocity threats, making defense systems safer and more effective. The current study utilizes a comprehensive numerical analysis to fill a critical research gap in this field. By studying factors such as material behavior, structural deformation, and failure modes of RC slabs, we aim to fill the knowledge gap that exists regarding their response to high-velocity projectile impacts. This study may contribute to guiding engineering practices, influencing design codes, and improving protective technologies in scenarios where projectile impact poses a significant risk. In pursuit of the study objective, we have formulated and fine-tuned a numerical model using the widely recognized finite element modeling technique. The model's accuracy has been confirmed through comparison with published experimental findings. Subsequently, the model results have been used to gain insights into the effects of high-velocity loading on RC slabs.

NUMERICAL MODELING

In this study, a finite element (FE) numerical model of RC slabs under high-velocity loading was created. The simulations were performed utilizing the LS-Dyna FE software (LS-DYNA R11.1.0), which is particularly well-suited for analyzing dynamic issues of this kind. The validity of the developed model was established by comparing its numerical outcomes with experimental test results from 15 specimens that were tested by other researchers. In this context, impact test simulations were conducted using a setup similar to the one documented by Hering et al. (Hering et al. 2020). Detailed information about the developed model and its performance capabilities are presented in the subsequent sections.

Creating the geometry, mesh, and interactions of the model

Geometry and discretization

In the current research, the comprehensive model consists of multiple elements, encompassing the concrete slab, reinforcement steel, impactor, load cells, and binders. The concrete portion of the designated slab was simulated using eight-node continuum hexahedron solid elements with the single integration element formulation. The steel reinforcement was explicitly represented using two-node beam elements, utilizing the default Hughes-Liu element formulation.

Table 1 Element details of the FE model.

Component	Element type	Number of elements	Number of nodes
Concrete, depth 100 mm	8-node solid	225,000	250,811
Concrete, depth 200 mm		450,000	478,821
Concrete, depth 300 mm		675,000	706,831
Impactor		35,420	37,518
Load cells		82,620	90,368
Binders		1,152	2,028
Reinforcement	2-node beam	16,240	32,536

In this context, the concrete section was discretized with a mesh size of 10 mm, while the reinforcement bars were discretized uniformly with a mesh size of 5 mm. The binders, load cells, and impactors were all simulated using eight-node solid elements. **Figure 1** illustrates the representative discretization for the reinforced concrete (RC) slab with a depth of 300 mm. A comprehensive breakdown of the elements and nodes constituting each component within each model is outlined in **Table 1**.

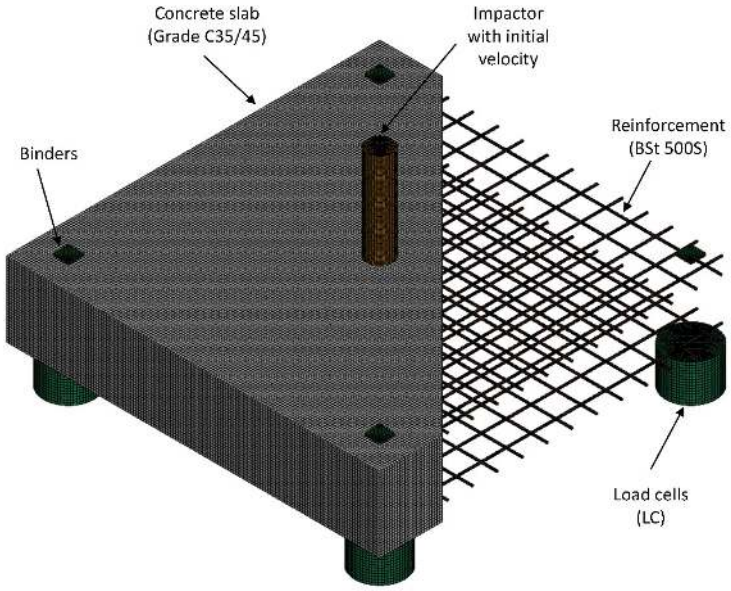

Figure 1 FE discretization of the model components.

Modeling steel-concrete contact and other interactions

In this study, the explicit modeling of reinforcement led to the adoption of the constraint node method, which effectively integrated the reinforcement bars into the continuous volume elements of the concrete. This integration was achieved through the implementation of the constrained beam in a solid algorithm, a feature available within LS-Dyna. Furthermore, interaction dynamics at the interface among the concrete, reinforcement, and impactor were established using the standard contact algorithm, employing an eroding surface-to-surface technique. This approach ensured ongoing interaction throughout the gradual penetration process of the impactor, even after the elimination of highly distorted elements (erosion elements). Additionally, interactions involving the binders, load cells, and the concrete slab were simulated using a frictional contact automatic surface-to-surface method.

Constitutive material models

A constitutive material model is a mathematical framework utilized to describe the behavior of a particular material under different loading conditions. These models exist in diverse forms, each designed to effectively capture the characteristics of different material types and loading scenarios. Here are the detailed characteristics of the material models applied to both concrete and steel.

In the case of each model, the process involves assigning the initial velocity denoted as v_{Imp} to the designated impactor node-set. This assignment is carried out using the LS-DYNA software, specifically by utilizing the keyword "initial velocity generation." Additionally, a precautionary measure is taken to ensure that the model remains immobile throughout the analysis. To achieve this, a set of actions is implemented. Firstly, the load cells, responsible for measuring forces or reactions, are subjected to constraints that restrict any potential movement they might otherwise undergo. This constraint applies across all directions, preventing any inadvertent shifts. Furthermore, the binders, which serve to hold components together, are also subjected to similar constraints, disallowing any form of movement in any conceivable direction. This comprehensive approach to immobilization guarantees that the model's structural integrity and intended analytical conditions are maintained without interference.

Concrete material model

The LS-Dyna finite element code provides a diverse range of material formulations that can be employed to characterize the mechanical behavior of concrete and cement-based composites subjected to impact loading. Previous research has extensively examined and evaluated various material models to ascertain their effectiveness in representing concrete's response under impact conditions, as explored in (Babiker 2021; Babiker et al. 2022). In light of this approach, the continuous surface cap model (*Mat 159), Schwer & Murray cap model (*Mat 145), and Karagozian & Case concrete model (*Mat 072R3) were considered as potential options. Among these options, the Schwer & Murray Cap Model (SMCM) was selected for this study due to its demonstrated high accuracy and the ease with which its material parameters can be adjusted to suit the specific requirements of the investigation.

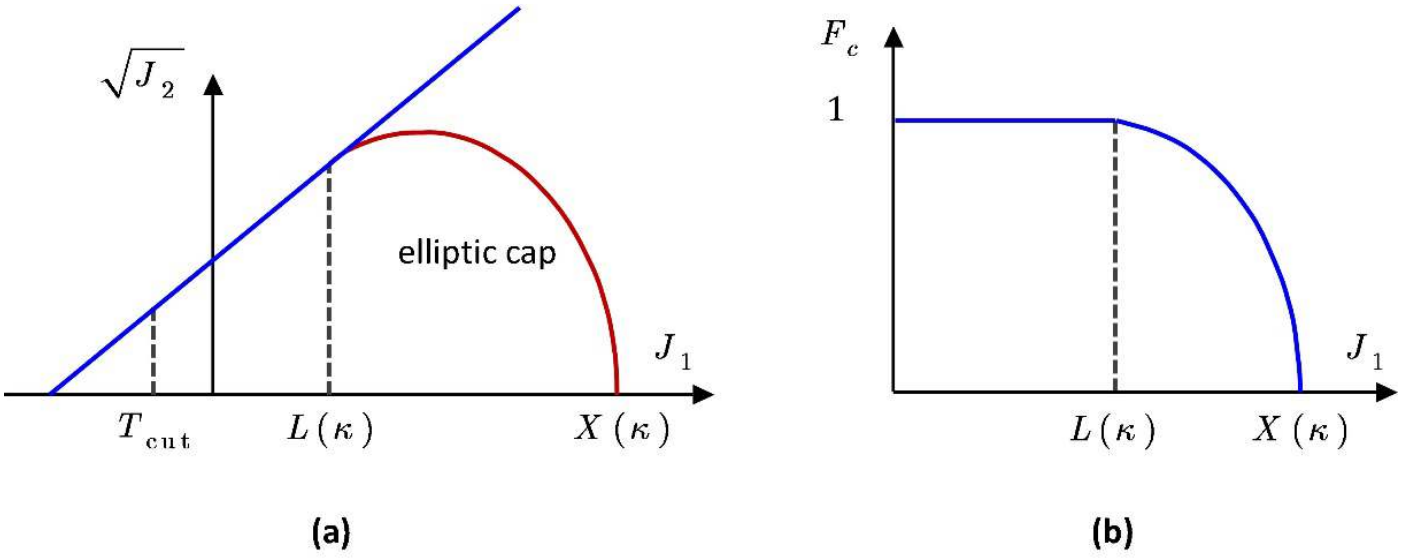

Figure 2 A schematic representation of the continuous surface cap model: (a) single surface smooth cap failure, and (b) non-dimensional function utilized with the cap portion of the smooth cap failure function.

The Schwer & Murray cap model (SMCM), developed by Schwer and Murray (Schwer and Murray 1994; 2002; Schwer 1994), is an extension of the Geologic cap model (*Mat 025) and incorporates three invariants. This formulation features a seamless failure surface and employs damage mechanics to account for strain softening and modulus degradation in both tension and compression. It also integrates viscoplasticity to address strain rate dependency (Jiang and Zhao 2015). An integral aspect of this model is the inclusion of an elliptical cap surface, which enables the effective representation of various geomaterials, encompassing soils, rocks, and concrete materials (LIVERMORE SOFTWARE TECHNOLOGY (LST) 2021). Furthermore, the model encompasses a unified

yield surface, consisting of a shear failure surface $F_f(J_1)$ and a cap surface $F_c(J_1,\kappa)$, interconnected continuously and smoothly, as depicted in **Figure 2**.

The shear failure of the smooth cap, depicted in **Figure 2 (a)**, can be mathematically expressed in relation to J_1 through an exponential function outlined in Eq. (1).

$$F_f(J_1) = \sqrt{J_2} = \alpha - \gamma \exp(-\beta J_1) + \theta J_1 \tag{1}$$

where, J_1 represent the first invariant of the stress tensor $J_1 = \sigma_{ii} = 3P$. The model parameters α, γ, β, and θ are employed to align experimental material data obtained in the laboratory.

The isotropic hardening behavior of the material formulation is contingent upon a non-dimensional function, illustrated in **Figure 2 (b)**, and can be represented by the expression provided in Eq. (2).

$$F_c(J_1,\kappa) = \begin{cases} 1, & J1 \le L(\kappa) \\ 1 - \dfrac{[J1 - L(\kappa)]^2}{[X(\kappa - L(\kappa))]^2}, & J1 > L(\kappa) \end{cases} \tag{2}$$

where κ is the hardening parameter used to control the movement of the cap surface, $L(\kappa)$ and $X(\kappa)$ define the shape of the cap surface, respectively. The function F_c equals one when J_1 is below $L(\kappa)$ and takes an elliptical form for $L(\kappa) \le J_1 \le X(\kappa)$.

To characterize the ellipticity of the cap surface, an additional parameter (material constant) denoted as R must be taken into account. This parameter is linked to the geometric parameters $L(\kappa)$ and $X(\kappa)$ in the following manner.

$$X(\kappa) = L(\kappa) + R\ F_f[L(\kappa)] \tag{3}$$

in which parameter $L(\kappa)$ is given by:

$$\kappa = \begin{cases} \kappa, & \kappa > \kappa_0 \\ \kappa_0, & \text{otherwise} \end{cases} \tag{4}$$

where k_0 is the value of J_1 at the initial intersection of the failure and cap surfaces.

The evolution of the cap's motion is governed by the rule of isotropic hardening, which can be expressed as given in Eq. (5).

$$\varepsilon_p^p = W\{1 - \exp(1 - D_1[X - X_0] - D_2[X - X_0]^2)\} \tag{5}$$

where $\varepsilon_p^p = \text{tr}\ \varepsilon_{ij}^p$ denotes the plastic volumetric strain, W represents the maximum plastic volumetric strain, X_0 is the initial abscissa intercept of the cap surface, D_1 and D_2 are shape factors.

The parameters $L_0 = L(\kappa_0) = \kappa_0$, $X_0 = X(\kappa_0)$, and R represent the material inputs based on laboratory data. The incorporation of strain softening and modulus reduction for the concrete is achieved through an isotropic damage formulation. Strain softening captures the decline in strength beyond the peak point, while modulus reduction accounts for the decrease in elastic modulus during cyclic loading. The damage criterion is derived from the approach proposed by Simo and Ju (Simo and Ju 1987), which entails assessing the rate of energy release linked to damage progression.

Table 2 Constitutive model coefficients for concrete of grade C35/45.

Coefficient	Acronym	Value
Mass density [kg/m^3]	RO	2240
Shear modulus [GPa]	SHEAR	12.916
Bulk modulus [GPa]	BULK	17.222
Gruneisen ratio	GRUN	0
Shock velocity parameter	SHOCK	0
Flag for pore collapse	PORE	1
Shear failure Parameter [GPa]	ALPHA	0.0195098
Shear failure Parameter	THETA	0.3195781
Shear failure [GPa]	GAMMA	0.0117587
Shear failure [GPa^{-1}]	BETA	16.132549
Dilatation damage mechanics	EFIT	0
Kinematic strain hardening	ALPHA	0
Kinematic strain hardening	CALPHA	0
Initial cap surface ellipticity [GPa^{-1}]	RO	1.977944
Initial cap surface for [GPa]	XO	0.130607
Material type	IROCK	1
Shear enhanced compaction	SECP	0
Ductile damage mechanics	AFIT	1
Ductile damage mechanics	BFIT	0.606
Ductile damage mechanics	RDAMO	0.0107763
Plastic volume strain [GPa^{-2}]	W	0.065
Plastic volume strain [GPa^{-1}]	D1	0.611
Plastic volume strain [GPa^{-1}]	D2	2.224
History variable	NPLOT	23
Maximum permitted strain increment	EPSMAX	0
Brittle damage mechanics	CFIT	1
Brittle damage mechanics	DFIT	34.969
Tensile failure stress [GPa]	TFAIL	0.00297
Failure Flag, failed element	FAILFG	1
Rounded vertices	DBEAT	0
Rounded vertices	DDELTA	0
Viscoplasticity relaxation time	VPTAU	0
Torsion scaling parameter	ALPHA1	8.20E-04
Torsion scaling parameter [GPa-1]	THETA1	0.0
Torsion scaling parameter	GAMMA1	2.410e-4
Torsion scaling parameter [GPa-1]	BETA1	6.758225
Tri-axial extension scaling parameter	ALPHA2	7.600e-4
Tri-axial extension scaling [GPa-1]	THETA2	0.0
Tri-axial extension scaling	GAMMA2	2.600e-4
Tri-axial extension scaling [GPa-1]	BETA2	5.8666859

The smooth cap model illustrated in **Figure 2 (a)** is achieved by multiplying the failure and hardening surface functions, resulting in a continuous derivative function represented as:

$$f(J_1, J_2, \kappa) = J_2 - F_f^2 F_c R_s \tag{6}$$

where $J_2 = \frac{1}{2} S_{ij} S_{ij}$ is the second invariant of the deviatoric stress tensor, $S_{ij} = \sigma_{ij} - P\delta_{ij}$ is the stress tensor, and R_s is the Rubin scaling function (Rubin 1991). The material parameters for C35/35 concrete grade were determined by utilizing the fitting method proposed by Jiang and Zhao (Jiang and Zhao 2015), which is based on the uniaxial compressive strength, f_c'. The estimated material parameters for C35/45 concrete grade are given in **Table 2**.

Reinforcing-steel material model

In comparison to concrete, the complexity of steel reinforcement is relatively straightforward. In structural analysis, steel reinforcement is often assumed to exhibit linear elastic behavior. Nevertheless, it can also be represented with either an elastic-perfectly plastic or an elastic-plastic hardening model (LIVERMORE SOFTWARE TECHNOLOGY (LST) 2021; Simo and Ju 1987). In this research, the mechanical properties for steel reinforcement were established using the Piecewise linear plasticity material formulation (*Mat 024) (LIVERMORE SOFTWARE TECHNOLOGY (LST) 2021). This formulation is an ideal plastic material model that combines elasticity with plasticity and allows for the utilization of the Mises yield criterion alongside associated plastic flow. In this formulation, the evolution of the yield surface is defined by a piecewise linear relationship between effective stress and effective plastic strain. For many metallic materials, this model can be simplified into a bilinear elastic-plastic stress-strain relationship, as depicted in **Figure 3**.

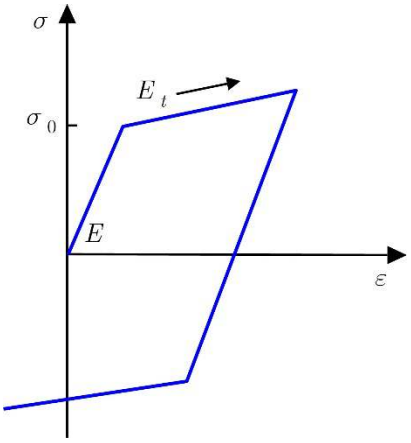

Figure 3 Elastic and plastic bilinear stress-strain curve with uniaxial geometry.

The Cowper-Symonds strength multiplier (Simo and Ju 1987) additionally offers the option of incorporating strain rate dependencies when necessary. This multiplier functions to amplify the material's yield strength as the effective plastic strain rate rises. The Cowper-Symonds multiplier can be adjusted using Eq. (7), wherein $\dot{\varepsilon}$ denotes the strain rate, while C and p represent the Cowper-Symonds constants. It is important to note that strain rate dependencies are not considered in this context. According to DIN 488-1 (DIN Deutsches Institut Für Normung 2009), the material parameters for BSt 500S are listed in **Table 3**.

$$\beta = 1 + \left(\frac{\dot{\varepsilon}}{C} \right)^{1/p} \tag{7}$$

Table 3 Constitutive model coefficients for BSt 500S steel.

Coefficient	Acronym	Value
Mass density [kg/m^3]	RO	7850
Elastic modulus [GPa]	E	210
Poisson's ratio [-]	PR	0.3
Yield stress [GPa]	SIG	0.5
Tangent modulus [GPa]	ETAN	0.0
Failure flag [-]	FAIL	0.165

Modeling approaches for load cells and binders

In this study, the load cells and support binders are considered to demonstrate linear elastic characteristics. As a result, their mechanical attributes were described utilizing LS-Dyna's Elastic material model (*Mat 001). The parameters required for each support in the simulation model are summarized in **Table 4**.

Table 4 Constitutive model coefficients of the binders and load cells.

Coefficient	Acronym	Value
Mass density [kg/m^3]	RO	7850
Elastic modulus [GPa]	E	210
Poisson's ratio [-]	PR	0.3

Verification of the formulated finite element model

In order to evaluate the precision of the formulated FE model and to establish a reliable basis for studying its behavior, the research turns to the experimental investigation carried out by (Hering et al. 2020) at the Otto Mohr Laboratory of Dresden University of Technology in Germany. This experimental initiative is leveraged to validate the accuracy of the developed FE model. Here, we provide a summarized overview of the particulars encompassing this experimental program.

The experimentation encompassed assessments performed on multiple RC slabs utilizing concrete of C35/45 grade. These slabs underwent testing within a high-energy accelerated drop tower apparatus, boasting a maximum drop height of 11 m, a drop mass reaching 2.5 tons, an unfettered fall energy equivalent to roughly 200 kJ, and an acceleration peaking at 160 m/s. The visual representation of the drop tower facility is illustrated in **Figure 4**. For in-depth insights, please refer to the works of (Just, M., Curbach, M., Kühn, T., & Hering, M. 2016) and (Hering et al. 2020; 2016).

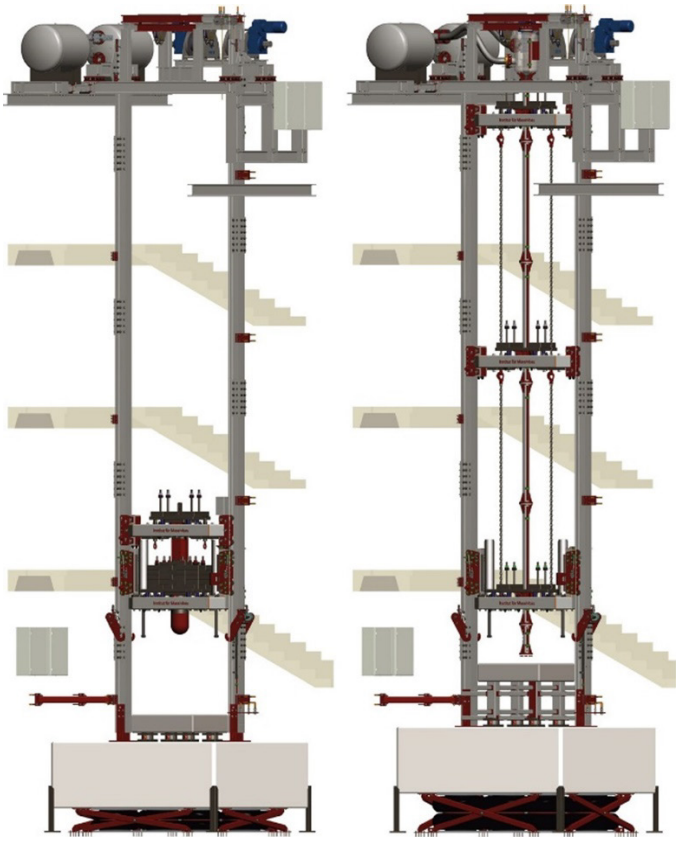

Figure 4 Schematic representation of Otto Mohr drop-tower apparatus: (left) free fall configuration, (right) accelerated configuration.

The tested reinforced concrete (RC) slabs were accurately made to possess dimensions of 1500 mm in length and 1500 mm in width, while establishing varying depths denoted as (t_{Slab}), of 100, 200, and 300 mm. Each slab underwent reinforcement through the inclusion of high-yield steel bars (BSt 500S) with an 8 mm diameter, deliberately positioned

both at the upper and lower sections of the slab's structure. As per the guidelines outlined in DIN 488-1 (DIN Deutsches Institut Für Normung 2009), it was anticipated that the reinforcing steel bars exhibited a yield strength reaching 500 MPa. The arrangement of the reinforcing bars adhered to a consistent spacing of 100 mm intervals. A concrete cover measuring 25 mm was deliberately maintained between the longitudinal reinforcement and both the upper and lower edges of the slabs. **Figure 5** illustrates a comprehensive depiction of the reinforcement arrangement and the geometric configuration of the RC slab.

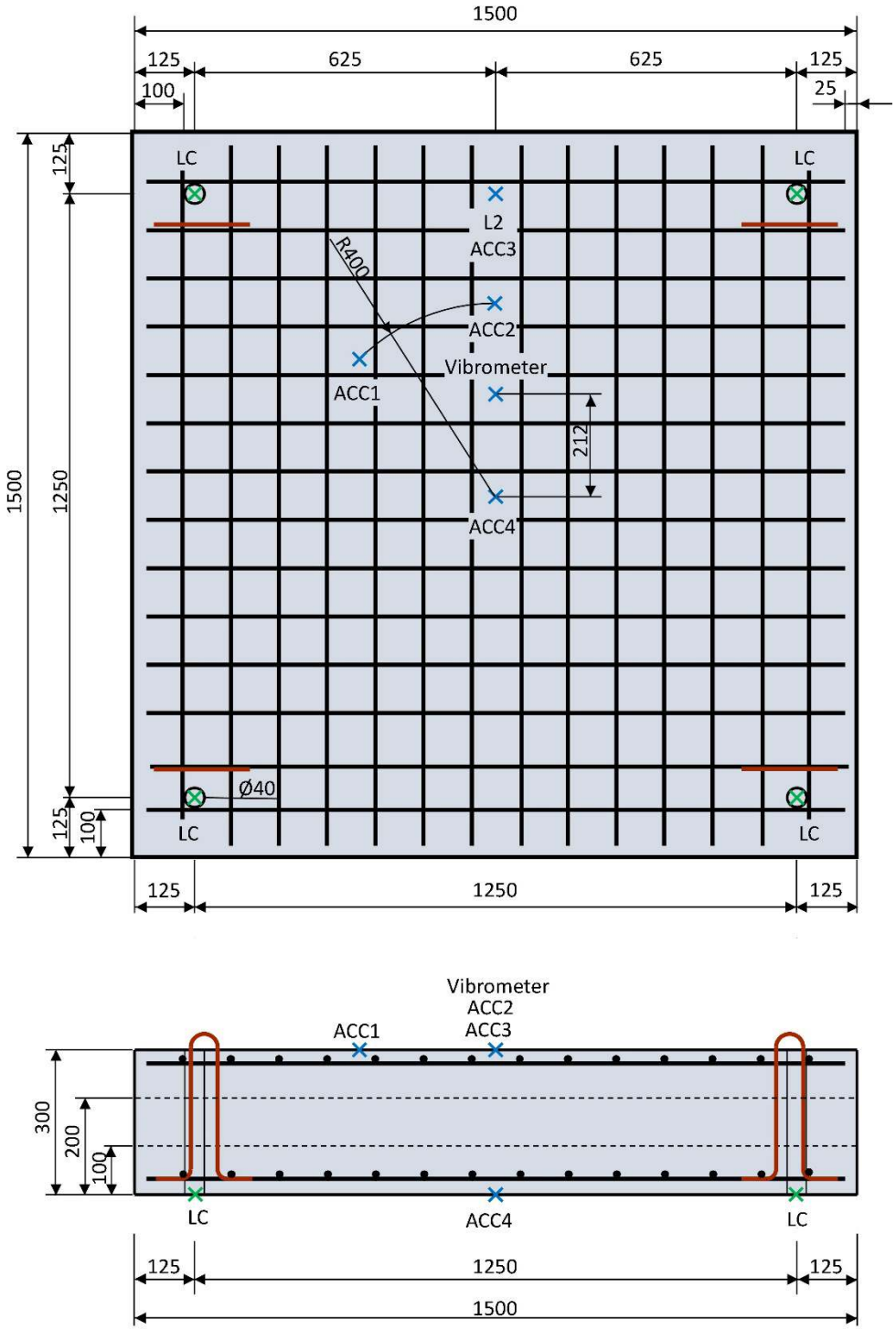

Figure 5 Slab's dimensions and arrangement of the reinforcing steel.

For all experiments, a cylindrical flat-nose impactor was utilized, featuring a diameter of 100 mm, a length measuring 380 mm, and an overall mass of 21.66 kg. The impactor is set in motion within the drop tower machine through a pipe,

and its velocity can be regulated by modifying the charge pressure of the machine. To investigate the impact characteristics and the resulting crack patterns causing damage to the RC slabs, various groups were subjected to testing under distinct impactor velocities. **Table 5** lists the tested RC slabs, their corresponding charge pressures, and the equivalent impactor velocities applied during the experiments.

Table 5 The details of the tested RC slabs.

Group	Slab ID	Slab depth t_{Slab} [mm]	Charge pressure [bar]	Impactor velocity v_{Imp} [m/s]
A	PL133	100	0.0	9.2
	PL132		0.0	12.7
	PL134		0.5	21.6
	PL131		1.0	26.1
	PL130		2.0	33.4
B	PL124	200	1.0	25.2
	PL121		2.0	32.7
	PL120		4.0	44.6
	PL122		6.0	53.9
	PL123		8.0	61.4
C	PL143	300	4.0	44.6
	PL140		6.0	54.5
	PL142		8.0	61.3
	PL141		10.0	68.4
	PL144		12.0	73.9

RESULTS AND DISCUSSION

Efficiency of the formulated finite element model

Analysis of reaction forces

Illustrated in **Table 1**, the subject slab is upheld at four distinct points, a design intended to serve a dual role: allowing for the assessment of both the support reactions and the deflections of the slab. The support reaction forces were individually gauged at every support point, referred to as LCs (Load Cells), and then aggregated to ascertain the comprehensive reaction forces exerted on the slab at each specific support position. **Figure 6** shows the computed support reactions for the three different investigated groups of slabs, analyzed across a wide range of impactor velocities. The experimental measurements are represented by dashed lines, while the additional details are summarized in **Table 6**. This table reveals that the developed model exhibited a relatively accurate prediction of the reaction forces, showing an average predicted-to-tested value ratio of approximately 71.3% and a coefficient of variation (COV) of 31.1%. Additionally, **Table 6** highlights that the developed model showcased a reasonably precise forecast of the displacements, demonstrating an average predicted-to-tested value ratio of roughly 1.18 and a COV amounting to 29.3%. The disparity observed between numerical reaction forces and their experimental counterparts can be attributed to various factors, notably the consistent algorithm employed at the interface between the load cells and the RC slab.

Upon a thorough examination of the simulation outcomes presented in **Figure 6(a)–(c)**, an obvious trend emerges the reaction force escalates in a cycle with the velocity of the impactor. This observed pattern concurs with the experimental findings, notably pronounced in the context of group B slabs, as highlighted in **Figure 6 (e)**. It is important to note, however, that this escalation in reaction force remains apparent only until the point of what is referred to as the "perforation limit," which, for group B slabs, resides between 54 and 61 m/s. In an overarching context, the simulated reaction forces exhibit a commendable degree of convergence with the experimental counterparts, particularly regarding their peak values, as explained in **Figure 6**. Nevertheless, for a more careful alignment with the experimental results, a deeper convergence may necessitate additional endeavors such as material calibration, discretization refinements, and other enhancements.

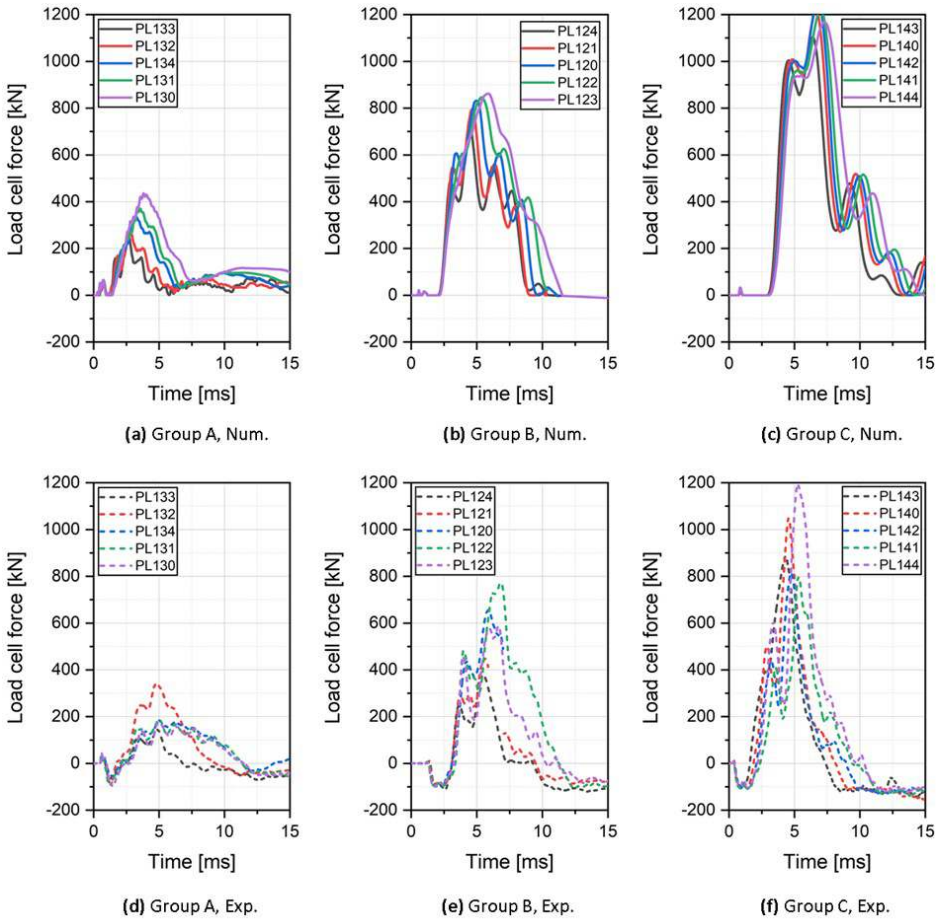

Figure 6 Reaction forces for varied slab depths.

Table 6 Summary of the experimental results.

Slab ID	Load cell force [kN]		$\frac{P_{Exp}}{P_{Num}}$	Slab displacement [mm]		$\frac{\delta_{Exp}}{\delta_{Num}}$
	Exp. P_{Exp}	Num. P_{Num}		Exp. δ_{Exp}	Num. δ_{Num}	
PL133	145.1	250.1	0.580	-3.5	-2.7	1.296
PL132	339.2	278.0	1.220	-5.4	-3.2	1.688
PL134	180.9	335.4	0.539	-6.8	-6.1	1.115
PL131	186.9	370.1	0.505	-5.5	-7.7	0.714
PL130	173.8	435.7	0.399	-5.7	-10.2	0.559
PL124	375.1	723.7	0.518	-3.9	-2.7	1.444
PL121	447.9	794.6	0.564	-4.7	-3.3	1.424
PL120	656.7	832.1	0.789	-6.3	-4.4	1.432
PL122	773.9	846.1	0.915	-7.1	-5.6	1.268
PL123	558.8	862.1	0.683	-4.4	-6.6	0.667
PL143	884.5	1103.9	0.801	-3.4	-2.7	1.259
PL140	1048.1	1209.9	0.866	-	-3.3	-
PL142	812.2	1264.6	0.642	-3.8	-3.6	1.056
PL141	795.12	1223.6	0.650	-6.1	-3.9	1.564
PL144	1192.7	1167.1	1.022	-4.3	-4.3	1.000
		μ	0.713			1.178
		σ [%]	22.204			34.462
		COV [%]	31.144			29.266

Note. μ : mean, σ : standard deviation, COV: coefficient of variance.

Analysis of displacement responses

Figure 7 illustrates the displacement-time profiles of the studied slabs, compared with the corresponding experimental outcomes. These profiles were extracted from the upper surface of the plate, specifically at the designated "Vibrometer" point located at a distance of 212 mm from the impact center, as depicted in **Figure 5**. Notably, an incremental rise in displacement amplitude is observed with the projectile velocity, culminating upon reaching the perforation limit.

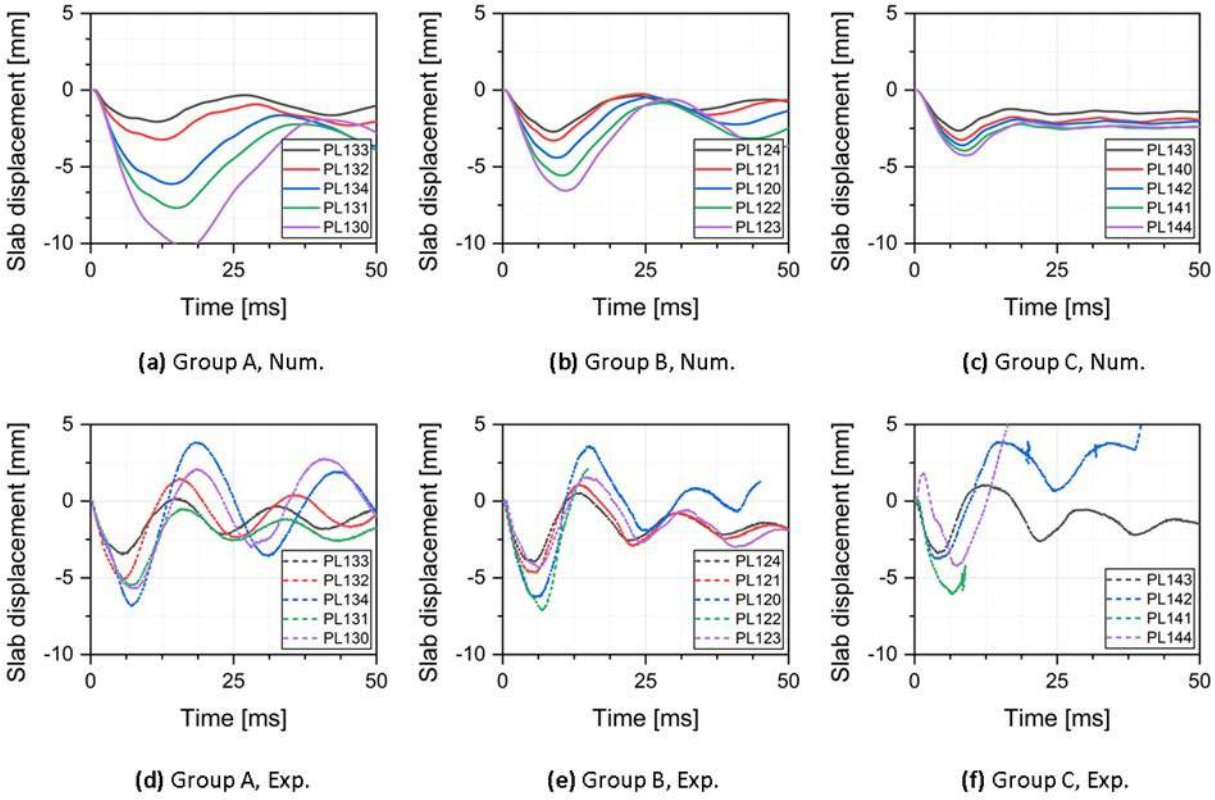

Figure 7 Slab displacements for varied slab depths.

It is of utmost importance to acknowledge that the calculation of slab displacement profiles was limited to a duration of 50 ms in order to optimize computational efficiency. Nevertheless, to ensure accurate measurements, particularly in the context of group A and B slabs, an extended simulation time of approximately 100 ms was deemed necessary. The aforementioned observations suggest that when compared to the experimental displacement profiles, the simulation results exhibit a level of agreement that can be considered generally acceptable.

Analysis of acceleration responses

To capture the accelerations of the slabs, an array of acceleration sensors labeled ACC1 to ACC4 were purposefully positioned on both the upper and lower surfaces of the slabs. The layout of these sensors is visibly presented in **Figure 5**. Remarkably, it is worth noting that among these sensors, only ACC4 was attached to the lower surface of the slab. The simulated acceleration profiles, calculated for the ACC1 and ACC2 sensor locations, are visually depicted in **Figure 8**, alongside their respective experimental measurements. Likewise, predictions for ACC3 and ACC4 are graphically portrayed in **Figure 9**.

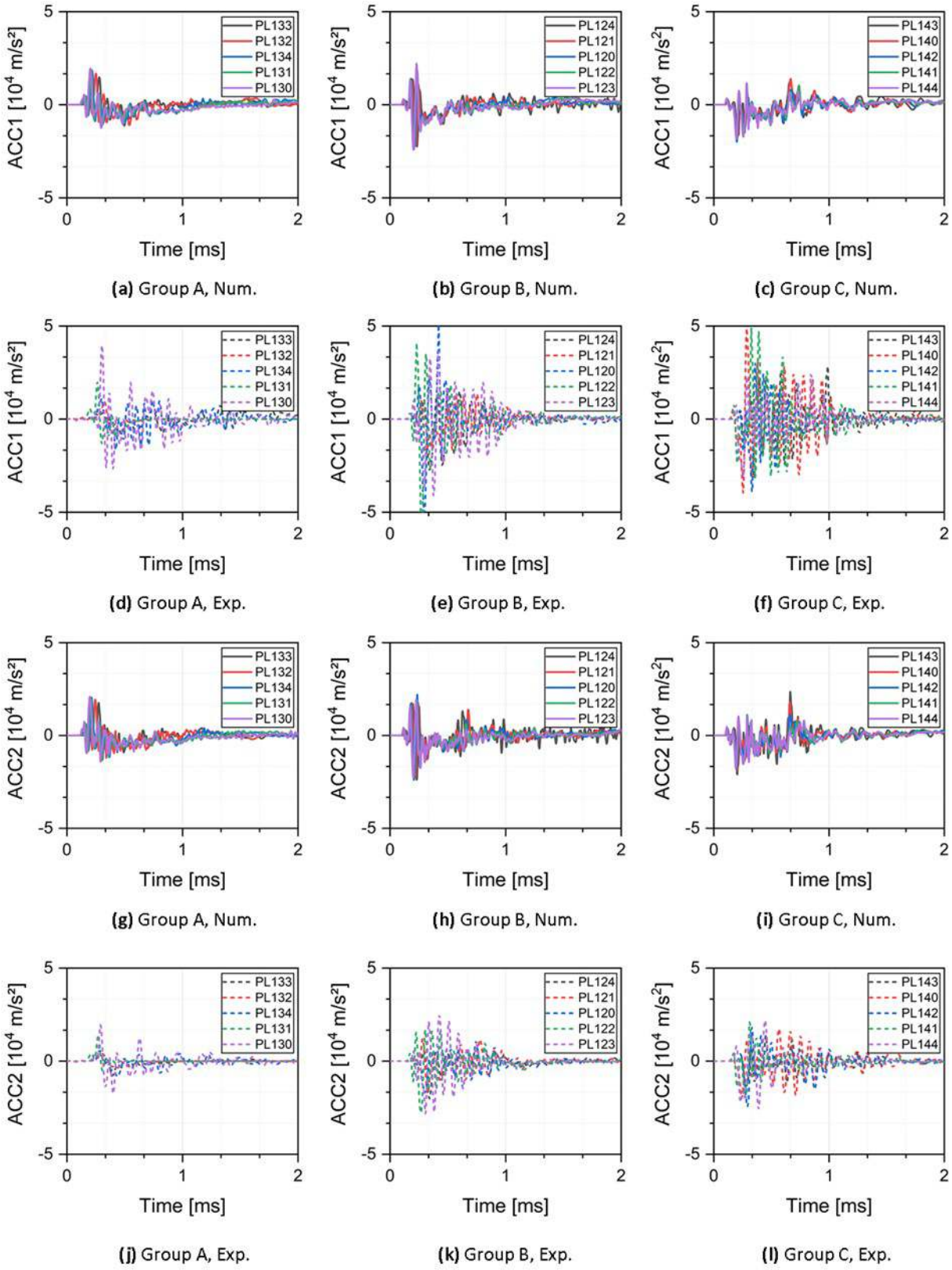

Figure 8 Slab accelerations for varied slab depths, ACC1 and ACC2.

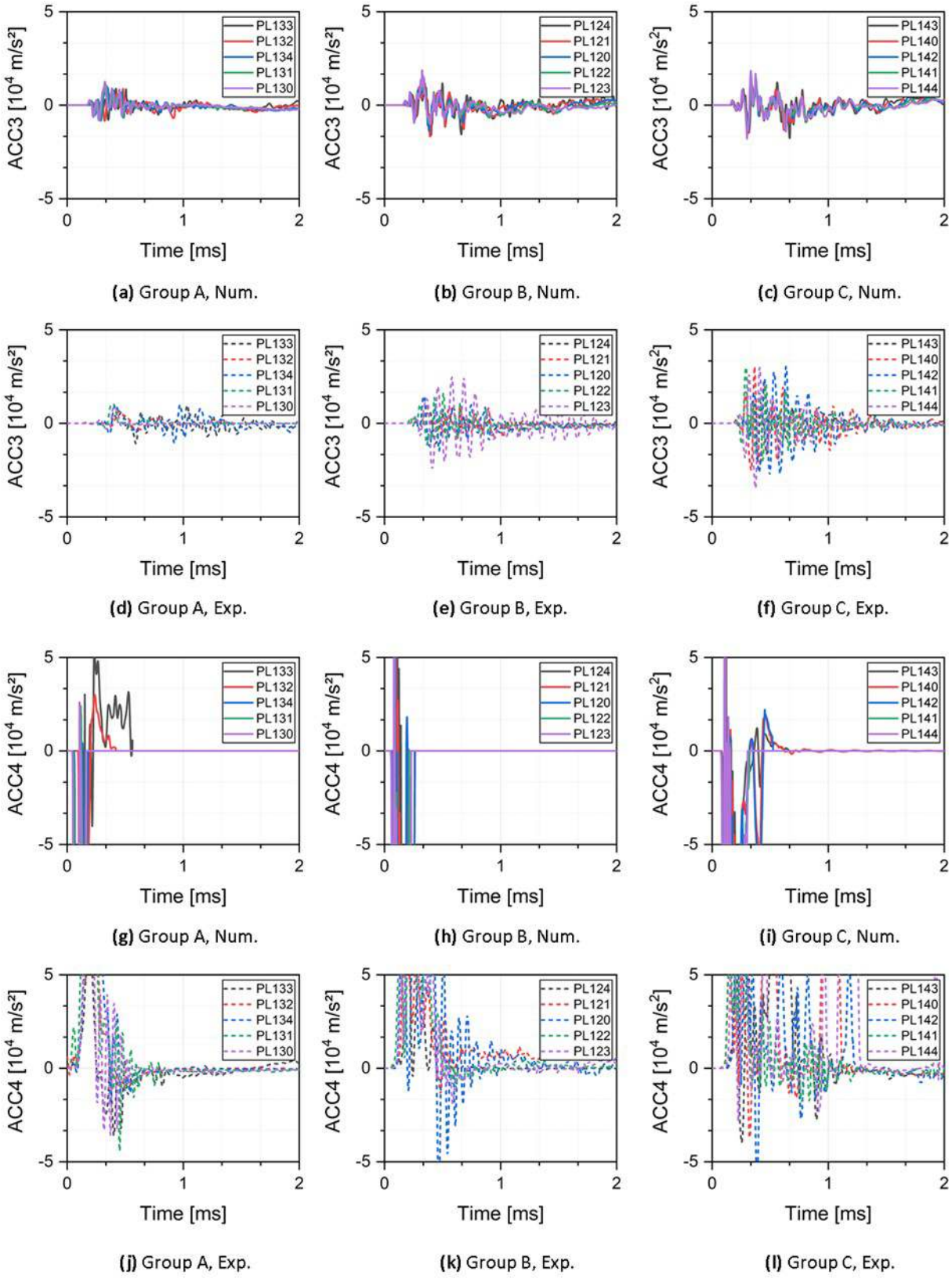

Figure 9 Slab accelerations for varied slab depths, ACC3 and ACC4.

In contrast to the trends observed in load cell forces, where their relationship with impact velocities shows a proportional increase, the behavior of acceleration is different. The acceleration doesn't exhibit a direct increase in magnitude as the impact velocity rises. This dissimilarity is significant, especially considering that the acceleration sensors ACC1 and ACC2 are both situated at an equidistant distance from the impact point, as depicted in **Figure 5**. Consequently,

the acceleration profiles computed at these sensors demonstrate nearly identical patterns. Nevertheless, it is essential to emphasize that the experimental measurements deviated from this consistent behavior.

Upon a thorough comparison between the numerical graphs illustrated in **Figure 8 (a), (b), and (c)** and their corresponding experimental plots depicted in **Figure 8 (d), (e), and (f)**, a noticeable discrepancy becomes evident. Specifically, the experimental acceleration measurements tend to exhibit an overestimation in relation to the numerical simulations. Consequently, a prudent recommendation would be to consider the utilization of acceleration sensors endowed with a narrower measurement range for enhanced accuracy.

Analysis of impact forces

Figure 10 displays the contact force, or impact force, exerted at the interface between the impactor and the target slabs. It's important to emphasize that these curves are absent from the experimental data, thus only the numerical results are provided for reference. Taking a look at **Figure 10**, it becomes apparent that, during initial contact between the impactor and the target slab, there is an impact force that is reminiscent of a half-sine wave during the initial impact phase. **Figure 10 (a)** shows that the peak contact force of 1809 kN for slabs in group A suddenly rises at 0.33 ms, and then falls as the speed of the impactor decreases, falling to 17.4 kN in approximately 8.91 ms. Similarly, for group B slabs (**Figure 10 (b)**) and group C slabs (**Figure 10 (c)**), the peak contact force is 3388.44 and 4273.13 kN, respectively.

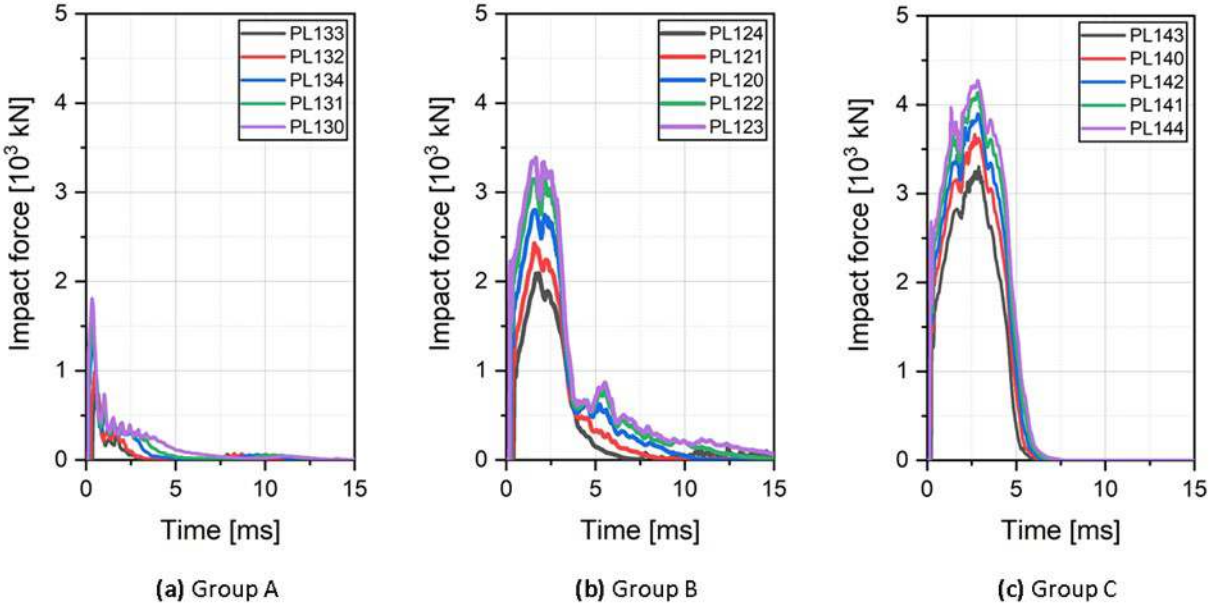

Figure 10 Impact forces for varied slab depths.

Analysis of impactor velocities

Figure 11 depicts a chronology of the impactor's velocity as it collides with the target slab from the moment of impact. This figure highlights the differing impactor dynamics at different velocities upon hitting the slabs. Based on the analysis of **Figure 11 (a)**, it can be seen that velocity has decreased rapidly over time. A similar trend is observed for the slabs in groups B and C, as shown in **Figure 11 (b)–(c)**. respectively. Additionally, the visual depictions furnished by **Figure 11** substantiate the previously expounded concept of the perforation limit. The congruence between these graphical representations and the previously addressed idea bolsters the comprehension that a distinct threshold exists, surpassing which results in the occurrence of perforation.

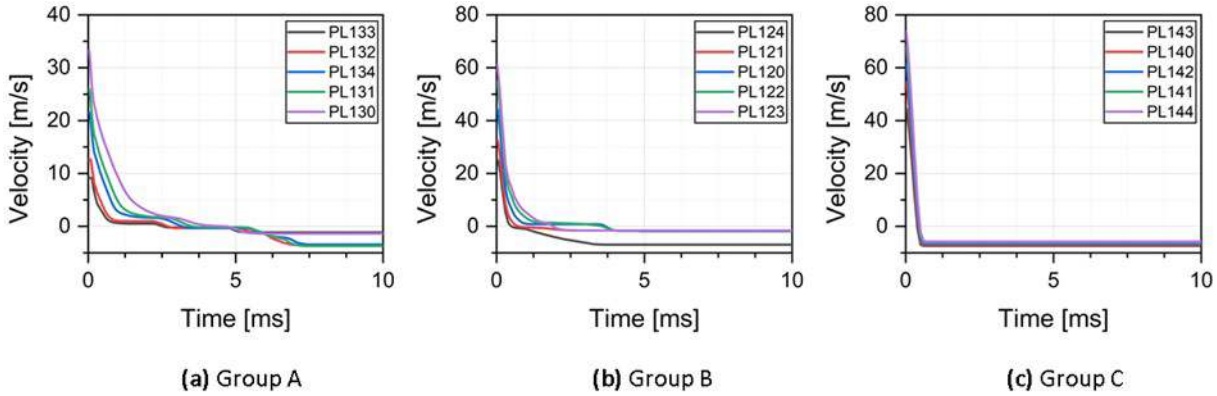

Figure 11 Variation of the impactor velocities during penetration.

Patterns of failure

In accordance with Kennedy's work (Kennedy 1976), the impact of a projectile on the target slab is expected to give rise to a range of distinct damage scenarios. These encompass spalling, projectile penetration, perforation, and concrete scabbing. In **Figure 12,** a comparative assessment of the final damage state, as deduced from experiments and analyses, is presented for the center cut plane of the investigated slabs. The observed failure of group A slabs, both in simulations and experimental observations, manifested as a combination of bending and shearing cone failure. As expected, the increment of projectile velocity led to a corresponding escalation in damage until the target slab was completely perforated. This consistent behavior was evident in both the analysis and experimental findings demonstrating the reliability of the chosen material models.

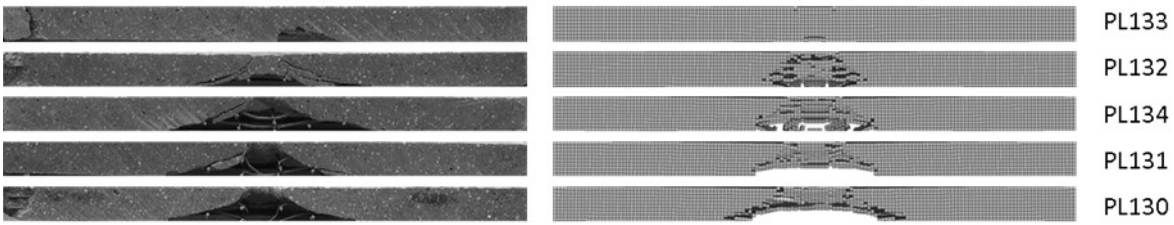

Figure 12 Final state failure pattern at the center of the slab cut plan: (left) experimental observation, and (right) numerical result, group A.

The crack patterns of group B and C slabs, observed through both experiments and numerical simulations, are in **Figure 13** and **Figure 14**, respectively. Upon comparing the experimental and numerical representations of damage for group B slabs, no significant distinctions are discernible.

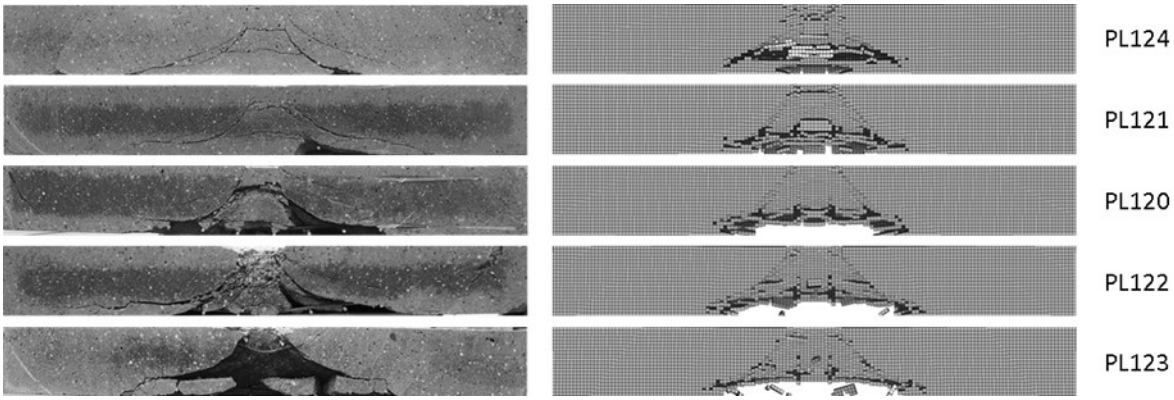

Figure 13 Final state failure pattern at the center of the slab cut plan: (left) experimental observation, and (right) numerical result, group B.

Across all five scenarios encompassing varying projectile velocities (ranging from 25.5 to 61.4 m/s), the extent of destruction is substantial enough to generate a conical punch that penetrates the slab's depth. However, unlike the cases of group A and B slabs, the fractured slabs within group C display slightly different behavior. In instances of low projectile

speeds (PL143 and PL40), only a very hard noticeable conical punch is observed in the experimental observations. This conical punch becomes notably more prominent at higher projectile speeds (PL142, PL141, and PL144). Nevertheless, this observation exhibits some divergence in the numerical results.

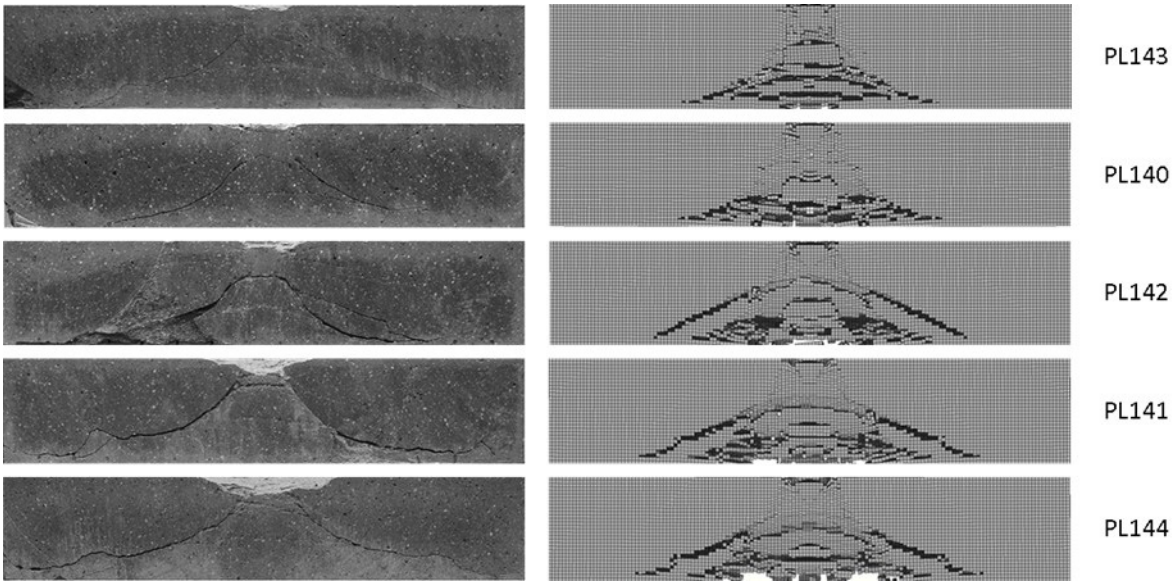

Figure 14 Final state failure pattern at the center of the slab cut plan: (left) experimental observation, and (right) numerical result, group C.

Response surface analysis

Proposed response surface formulation

In this investigation, a straightforward analytical framework was formulated to forecast the load-carrying capability (p_u) and the accompanying deflection (δ_m) of a slab subjected to high-velocity loads. This framework was crafted utilizing the preceding experimental data from Table 5 and Table 6 and harnessed the capabilities of a versatile statistical software program [Minitab (Rinaman 1959) (version 19.0)].

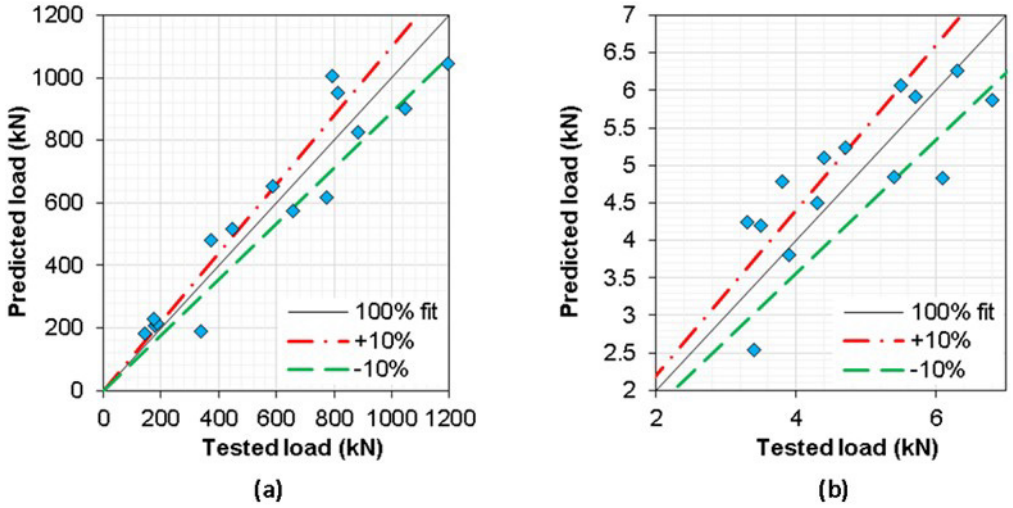

Figure 15 Predicted vs. tested results: (a) p_u , and (b) δ_m .

The autonomous factors of the model were the slab's thickness (x_2) and the impactor velocity (x_1). Here, the model was constructed utilizing a fully crossed design element, which facilitates the exploration of both the singular effects of individual parameters on an independent variable and the repercussions arising from interactions among dependent variables. This analysis has yielded the formulation of two models as presented in Eqs. (8)–(9). Both analytical approaches

have exhibited satisfactory performance, as evidenced by their coefficient of correlation presented in these equations. This reasonable predictive accuracy is also demonstrated in **Figure 15**, where the calculated results are compared to the tested data. This figure illustrates that a significant portion of the tested-to-predicted values exhibited proximity within a ±10% error margin.

$$P_u = -101 + 3.02x_1 - 0.9x_2 - 0.0037x_1^2 - 0.005x_2^2 + 0.03x_1x_2 \quad (R^2 = 0.64) \tag{8}$$

$$\delta_m = 3.84 + 0.0076x_1 + 0.098x_2 - 0.00027x_1^2 - 0.0054x_2^2 + 0.0203x_1x_2 \quad (R^2 = 0.64) \tag{9}$$

Isoresponses of slabs subjected to high-velocity loading

The formulation of the earlier response surface-based model [Eqs. (8)–(9)] facilitates the creation of response contours, offering a deeper understanding of how different parameters influence the response surface. The outcomes of this analysis are displayed in **Figure 16** and **Figure 17**. These figures can be used to design RC slabs that can withstand different impact scenarios. **Figure 16** shows how the impactor velocity and the thickness affect the load of a RC slab. The figure shows that for a fixed thickness, the load will likely increase as the impactor velocity decreases. This means that the slab material can resist higher loads by slowing down the impactor more. This result is consistent with some previous research on the impact behavior of RC slabs. For example, Yilmaz et al. (Yılmaz et al. 2020) found that the impact load decreased as the impactor velocity decreased for RC slabs with different support types. Similarly, Al-Dala'ien et al. (Al-Dala'ien et al. 2023) reported that the impact load decreased as the impactor velocity decreased for RC slabs with different reinforcement ratios.

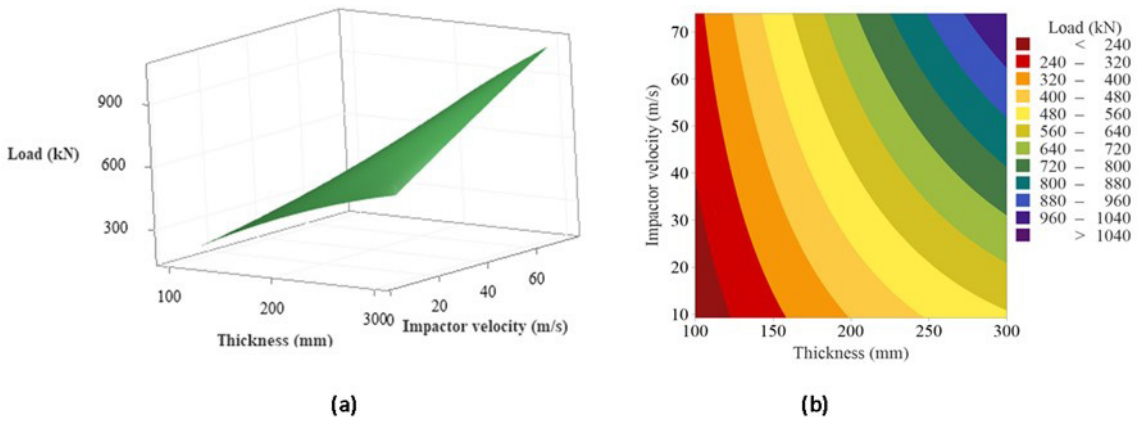

Figure 16 Load: (a) response surface, and (b) contours isoresponses.

Moreover, **Figure 17** depicts the contour plots of impactor velocity vs. thickness with displacement. From the figure, it can be seen the likelihood of displacement increases with the impactor velocity. This means that the slab is more likely to deform when it is hit by a faster impactor. Additionally, the displacement also seems to have a nonlinear relationship with both variables. It is noteworthy that this finding is consistent with the results of Liu et al. (H. Liu et al. 2020), who studied the low-velocity impact behavior of fiber-reinforced composites using two types of impactors: a hemispherical head and a flat-ended one. These investigators concluded that the damaged area and depth increased with both the impact energy and the thickness of the composite specimens. They also observed a nonlinear relationship between these variables, as the damage growth rate was higher for higher energy levels and thicker specimens.

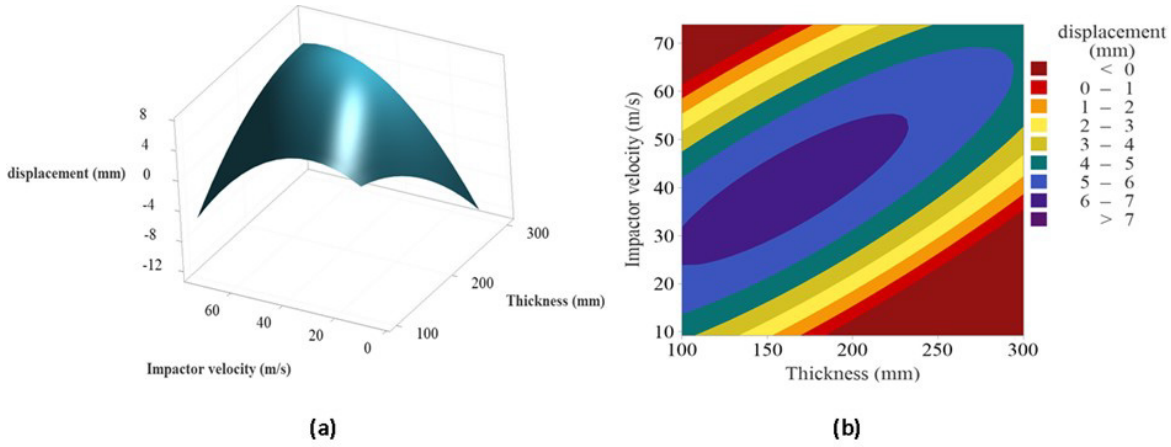

Figure 17 Deflection: (a) response surface, and (b) contours isoresponses.

CONCLUSION

The present study was focused on investigating the dynamic response of RC slabs when subjected to high-velocity projectile impacts. The primary objective was to assess the influence of varying levels of impact loading and slab depths on these structures, utilizing numerical simulations and response surface analysis techniques. Elaborate numerical models were meticulously constructed and simulated using the LS-Dyna explicit finite element software. Initial emphasis was placed on comprehending the rate-dependent behavior of RC slabs under impact conditions. To achieve this, the developed models underwent a range of impactor velocities, enabling in-depth exploration of failure patterns, damage severity, impact forces at the interface between the impactor and slab, reaction forces at the interface between the load cell and slab, as well as slab accelerations and vertical displacements. These simulations were enriched with experimental data, which validated the simulation outcomes by exhibiting a commendable alignment with corresponding experimental findings. Furthermore, a straightforward analytical framework was established to predict the load-carrying capacity and deflection of slabs exposed to high-velocity loads. Based on the findings of this study, the following conclusions were drawn:

1. The chosen material models and contact algorithms within LS-Dyna effectively captured experimental behavior across a spectrum of impact loading rates. However, achieving a more precise agreement between the finite element (FE) model and experimental results may necessitate additional efforts, including fine-tuning material calibration, refining discretization, and implementing other enhancements.
2. Both analytical approaches demonstrated satisfactory performance, with a significant portion of predicted values closely aligned within a ±10% error margin.
3. The response surface analysis highlighted that, for a fixed thickness, the load is expected to increase as impactor velocity decreases. This implies that the slab material can withstand higher loads by decelerating the impactor. Moreover, the displacement exhibited a nonlinear relationship with both slab thickness and impactor velocity.
4. The finite element analysis has proven invaluable in providing insights into material complexities and is deemed essential for achieving a profound understanding and accurate outcomes in specific material scenarios. The study's outcomes shed light on the intricate dynamics of RC slabs subjected to high-velocity impacts, offering valuable implications for structural design and analysis.

ACKNOWLEDGEMENTS

The authors extend their appreciation to Researcher Supporting Project number (RSPD2024R692), King Saud University, Riyadh, Kingdom of Saudi Arabia.

Author's Contributions: Conceptualization, A. Babiker and Y. M. Abbas; Methodology, A. Babiker, Y. M. Abbas and M. I. Khan; Investigation, A. Babiker and Y. M. Abbas; Writing - original draft, A. Babiker, Y. M. Abbas; Writing - review & editing, A. Babiker, Y. M. Abbas and M. I. Khan; Software, A. Babiker; Visualization, A. Babiker and Y. M. Abbas.

Editor: Marcílio Alves

References

Al-Dala'ien, Rayeh Nasr, Agusril Syamsir, Mohd Supian Abu Bakar, Fathoni Usman, and Mohammed Jalal Abdullah. 2023. "Failure Modes Behavior of Different Strengthening Types of RC Slabs Subjected to Low-Velocity Impact Loading: A Review." *Journal of Composites Science* 7 (6). https://doi.org/10.3390/jcs7060246.

Andrew, J. Jefferson, Sivakumar M. Srinivasan, A. Arockiarajan, and Hom Nath Dhakal. 2019. "Parameters Influencing the Impact Response of Fiber-Reinforced Polymer Matrix Composite Materials: A Critical Review." *Composite Structures*. https://doi.org/10.1016/j.compstruct.2019.111007.

Babiker, Ammar. 2021. "Numerical Modeling of Steel Fiber Reinforced Concrete Composite Exposed to High Loading Rate." Fakultät Bauingenieurwesen, Technische Universität Dresden. https://tud.qucosa.de/landing-page/?tx_dlf[id]=https%3A%2F%2Ftud.qucosa.de%2Fapi%2Fqucosa%253A74496%2Fmets.

Babiker, Ammar, Aamir Dean, Ebtihag Abu-Elgasim, and Taghried Abdel-Magid. 2022. "Numerical Modeling of Steel Fiber Reinforced Concrete Spallation Exposed to Medium Loading Rate." *Global Journal of Engineering and Technology Advances* 12 (2): 001–014. https://doi.org/10.30574/gjeta.2022.12.2.0130.

Bencardino, Francesco, Antonio Condello, and Ashraf F. Ashour. 2017. "Single-Lap Shear Bond Tests on Steel Reinforced Geopolymeric Matrix-Concrete Joints." *Composites Part B: Engineering* 110. https://doi.org/10.1016/j.compositesb.2016.11.005.

Bruhl, Jakob C., Amit H. Varma, and William H. Johnson. 2015. "Design of Composite SC Walls to Prevent Perforation from Missile Impact." *International Journal of Impact Engineering* 75: 75–87. https://doi.org/10.1016/j.ijimpeng.2014.07.015.

Cadoni, Ezio, Matteo Dotta, Daniele Forni, Nicoletta Tesio, and Carlo Albertini. 2013. "Mechanical Behaviour of Quenched and Self-Tempered Reinforcing Steel in Tension under High Strain Rate." *Materials and Design* 49. https://doi.org/10.1016/j.matdes.2013.02.008.

Chandran, Sarath, Wenqi Liu, Junhe Lian, Sebastian Münstermann, and Patricia Verleysen. 2022. "Strain Rate Dependent Plasticity and Fracture of DP1000 Steel under Proportional and Non-Proportional Loading." *European Journal of Mechanics, A/Solids* 92. https://doi.org/10.1016/j.euromechsol.2021.104446.

Chen, X. W., X. L. Li, F. L. Huang, H. J. Wu, and Y. Z. Chen. 2008. "Normal Perforation of Reinforced Concrete Target by Rigid Projectile." *International Journal of Impact Engineering* 35 (10): 1119–29. https://doi.org/10.1016/j.ijimpeng.2008.01.002.

Chen, X.W., X. L. Li, F. L. Huang, H. J. Wu, and Y. Z. Chen. 2007. "Modeling of Normal Perfolation of Reinforced Concrete Slab by Rigid Projectile." *23Rd International Symposium on Ballistics*, no. April: 1235–42.

Dancygier, Avraham N. 1997. "Effect of Reinforcement Ratio on the Resistance of Reinforced Concrete to Hard Projectile Impact." *Nuclear Engineering and Design* 172 (1–2): 233–45. https://doi.org/10.1016/s0029-5493(97)00055-1.

Daudeville, Laurent, and Yann Malécot. 2011. "Concrete Structures under Impact." *European Journal of Environmental and Civil Engineering* 15 (January): 101–40. https://doi.org/10.1080/19648189.2011.9695306.

Deng, Bo Yu, Xin Liu, Ke Quan Yu, Ling Zhi Li, and Yu Chen. 2022. "Seismic Retrofitting of RC Joints Using Steel Cage and Haunch with Bolted Steel Plate." *Structures* 43. https://doi.org/10.1016/j.istruc.2022.06.056.

Dhiman, P., Kumar, V. 2023. "Numerical Investigation of Reinforced Concrete Beams under Impact Loading." *Asian Journal of Civil Engineering* 1 (18). https://doi.org/10.1007/s42107-023-00793-0.

DIN Deutsches Institut Für Normung, C. 2009. *DIN488-1 Reinforcing Steels - Part 1: Grades, Properties, Marking*. http://arxiv.org/abs/1011.1669%0Ahttp://dx.doi.org/10.1088/1751-8113/44/8/085201.

Erzar, B., and P. Forquin. 2011. "Experiments and Mesoscopic Modelling of Dynamic Testing of Concrete." *Mechanics of Materials* 43 (9): 505–27. https://doi.org/10.1016/j.mechmat.2011.05.002.

Fan, Wei, Zhengwu Zhong, Xu Huang, Wenbiao Sun, and Wei Mao. 2022. "Multi-Platform Simulation of Reinforced Concrete Structures under Impact Loading." *Engineering Structures* 266. https://doi.org/10.1016/j.engstruct.2022.114523.

Gomathi, K. Akshaya, A. Rajagopal, K. S.S. Reddy, and B. Ramakrishna. 2020. "Plasticity Based Material Model for Concrete Subjected to Dynamic Loadings." *International Journal of Impact Engineering* 142 (April): 103581. https://doi.org/10.1016/j.ijimpeng.2020.103581.

Hao, Y. F., X. H. Zhang, and H. Hao. 2011. "Numerical Analysis of Concrete Material Properties at High Strain Rate under Direct Tension." *Procedia Engineering* 14 (1): 336–43. https://doi.org/10.1016/j.proeng.2011.07.042.

Hering, Marcus, Franz Bracklow, Tino Kühn, and Manfred Curbach. 2020. “Impact Experiments with Reinforced Concrete Plates of Different Thicknesses.” *Structural Concrete* 21 (2): 587–98. https://doi.org/10.1002/suco.201900195.

Hering, Marcus, and Manfred Curbach. 2018. “A New Testing Method for Textile Reinforced Concrete under Impact Load.” In *MATEC Web of Conferences*. https://doi.org/10.1051/matecconf/201819911010.

Hering, Marcus, Tino Kühn, Manfred Curbach, and Ulrich Häußler-combe. 2016. “Reinforced Concrete Slabs Under Impact – Scale Effects.” *Performance-Based Approaches for Concrete Structures Proc. of the Fib Symposium 21*: 23.

Jiang, Hua, and Jidong Zhao. 2015. “Calibration of the Continuous Surface Cap Model for Concrete.” *Finite Elements in Analysis and Design* 97: 1–19. https://doi.org/10.1016/j.finel.2014.12.002.

Just, M., Curbach, M., Kühn, T., & Hering, M. 2016. “Abschlussbericht / Final Report Bauteilverhalten Unter Stoßartiger Beanspruchung Durch Aufprallende Behälter (Flugzeugtanks) .” Dresden. https://doi.org/10.2314/GBV:868615218.

Karagöz İşleyen, Ümmü, Rahim Ghoroubi, Ömer Mercimek, Özgür Anıl, and R. Tuğrul Erdem. 2023. “Investigation of Impact Behavior of Glulam Beam Strengthened with CFRP.” *Structures* 51. https://doi.org/10.1016/j.istruc.2023.03.038.

Kennedy, R.P. 1976. “A Review of Procedures for the Analysis and Design of Concrete Structures to Resist Missile Impact Effects.” *Nuclear Engineering and Design* 37 (2): 183–203. https://doi.org/10.1016/0029-5493(76)90015-7.

Korucu, Hasan, and Ayhan Irfanoglu. 2018. “Response of Reinforced Concrete Beams to High-Velocity Fluid Impact. Part II: Numerical Modeling and Simulation.” *Structural Concrete* 19 (4): 1115–21. https://doi.org/10.1002/suco.201600164.

Liu, Haibao, Jun Liu, Yuzhe Ding, Jin Zhou, Xiangshao Kong, Bamber R.K. Blackman, Anthony J. Kinloch, Brian G. Falzon, and John P. Dear. 2020. “Effects of Impactor Geometry on the Low-Velocity Impact Behaviour of Fibre-Reinforced Composites: An Experimental and Theoretical Investigation.” *Applied Composite Materials* 27 (5). https://doi.org/10.1007/s10443-020-09812-8.

Liu, Jian, Ziqi He, Pengfei Liu, Jie Wei, Jun Li, and Chengqing Wu. 2023. “High-Velocity Projectile Impact Resistance of Reinforced Concrete Slabs with Ultra-High Performance Concrete Strengthening - A Numerical Study.” *Structures* 52. https://doi.org/10.1016/j.istruc.2023.03.174.

LIVERMORE SOFTWARE TECHNOLOGY (LST), AN ANSYS COMPANY. 2021. *LS-DYNA KEYWORD USER’S MANUAL - VOLUME II Material Models*. Vol. II. California: Livermore Software Tech. Comp. (LST), an Ansys Comp. www.lstc.com.

Lu, Gang, Xibing Li, and Kejin Wang. 2012. “A Numerical Study on the Damage of Projectile Impact on Concrete Targets.” *Computers and Concrete* 9 (1): 21–33. https://doi.org/10.12989/cac.2012.9.1.021.

Othman, H., and H. Marzouk. 2017. “Finite-Element Analysis of Reinforced Concrete Plates Subjected to Repeated Impact Loads.” *Journal of Structural Engineering* 143 (9). https://doi.org/10.1061/(asce)st.1943-541x.0001852.

Quan, X, N K Birnbaum, M S Cowler, B I Gerber, R A Clegg, and C J Hayhurst. 2003. “Numerical Simulation of Structural Deformation under Shock and Impact Loads Using a Coupled Multi-Solver Approach.” *Proceedings of 5th Asia-Pacific Conference on Shock and Impact Loads on Structures*.

Richard, Benjamin, Stefano Cherubini, François Voldoire, Pierre Etienne Charbonnel, Thierry Chaudat, Salim Abouri, and Nicolas Bonfils. 2016. “SMART 2013: Experimental and Numerical Assessment of the Dynamic Behavior by Shaking Table Tests of an Asymmetrical Reinforced Concrete Structure Subjected to High Intensity Ground Motions.” *Engineering Structures* 109. https://doi.org/10.1016/j.engstruct.2015.11.029.

Rinaman, WC and Minitab, In. 1959. *Revival: The Handbook of Software for Engineers and Scientists*. Vol. 2018. CRC Press: Boca Raton, FL, USA.

Rubin, M. B. 1991. “Simple, Convenient Isotropic Failure Surface.” *Journal of Engineering Mechanics* 117 (2): 348–69. https://doi.org/10.1061/(ASCE)0733-9399(1991)117:2(348).

Sahani, Ashok Kumar, and Amiya Kumar Samanta. 2022. “Bond Slip Behaviour of Deformed Bar Embedded in Sustainable Concrete at Elevated Temperature.” *Sadhana - Academy Proceedings in Engineering Sciences* 47 (2). https://doi.org/10.1007/s12046-022-01856-9.

Schwer, Leonard E. 1994. “Viscoplastic Augmentation of the Smooth Cap Model.” *Nuclear Engineering and Design* 150 (2–3): 215–23. https://doi.org/10.1016/0029-5493(94)90138-4.

Schwer, Leonard E., and Yvonne D. Murray. 1994. “A Three-invariant Smooth Cap Model with Mixed Hardening.” *International Journal for Numerical and Analytical Methods in Geomechanics* 18 (10): 657–88. https://doi.org/10.1002/nag.1610181002.

Schwer, Leonard E, and Yvonne D Murray. 2002. “Continuous Surface Cap Model for Geomaterial Modeling: A New LS-DYNA Material Type.” In *7th International LS-DYNA Users Conference, Material Technology (2)*, 35–50.

Simo, J. C., and J. W. Ju. 1987. “Strain- and Stress-Based Continuum Damage Models-I. Formulation.” *International Journal of Solids and Structures*. https://doi.org/10.1016/0020-7683(87)90083-7.

Tai, Y. S., T. L. Chu, H. T. Hu, and J. Y. Wu. 2011. “Dynamic Response of a Reinforced Concrete Slab Subjected to Air Blast Load.” *Theoretical and Applied Fracture Mechanics* 56 (3): 140–47. https://doi.org/10.1016/j.tafmec.2011.11.002.

Vijay, T.J., M. Manoj Kumar, G. Sofia, and R. Abiraami. 2020. “Impact Behaviour of Reinforced Concrete Slabs Embedded with Inclined Reinforcements.” *Materials Today: Proceedings*, 2. https://doi.org/10.1016/j.matpr.2020.09.360.

Yılmaz, Tolga, Nevzat Kıraç, Özgür Anil, R. Tuğrul Erdem, and Gökhan Kaçaran. 2020. “Experimental Investigation of Impact Behaviour of RC Slab with Different Reinforcement Ratios.” *KSCE Journal of Civil Engineering* 24 (1). https://doi.org/10.1007/s12205-020-1168-x.

Zhang, Xin, Zhen Jun Yang, Yu Jie Huang, Zhen Yu Wang, and Xiao Wei Chen. 2021. “Micro CT Image-Based Simulations of Concrete under High Strain Rate Impact Using a Continuum-Discrete Coupled Model.” *International Journal of Impact Engineering* 149. https://doi.org/10.1016/j.ijimpeng.2020.103775.